Wind and Structures, Vol. 11, No. 5 (2008) 345-359
DOI: http://dx.doi.org/10.12989/was.2008.11.5.345

Flow structures around a three-dimensional rectangular body with ground effect

Cahit Gurlek, Besir Sahin*, Coskun Ozalp and Huseyin Akilli

Cukurova University, Faculty of Engineering and Architecture,
Department of Mechanical Engineering, 01330 Adana, Turkey

(Received October 16, 2007, Accepted July 21, 2008)

Abstract. An experimental investigation of the flow over the rectangular body located in close proximity to a ground board was reported using the particle image velocimetry (PIV) technique. The present experiments were conducted in a closed-loop open surface water channel with the Reynolds number, $Re_H = 1.2\times10^4$ based on the model height. In addition to the PIV measurements, flow visualization studies were also carried out. The PIV technique provided instantaneous and time-averaged velocity vectors map, vorticity contours, streamline topology and turbulent quantities at various locations in the near wake. In the vertical symmetry plane, the upperbody flow is separated from the sharp top leading edge of the model and formed a large reverse flow region on the upper surface of the model. The flow structure downstream of the model has asymmetric double vortices. In the horizontal symmetry plane, identical separated flow regions occur on both vertical side walls and a pair of primary recirculatory bubbles dominates the wake region.

Keywords: ground vehicle aerodynamics; PIV, rectangular body; wake flow.

1. Introduction

The flow around a bluff body is of great interest in engineering applications such as determination of wind loads on buildings, heat transfer of electronic equipments or the simulation of the flow around vehicles. Understanding of the aerodynamic characteristics of road vehicles such as drag, lift, side forces, wind noise, stability and the accumulation of the water and dirt could lead improving the vehicle performance directly. Most previous studies used simplified vehicle models in order to understand the fundamental flow characteristics associated with more complex passenger vehicles.

The best known simplified vehicle-like shape named as Ahmed body, has been previously studied both experimentally and numerically. A near-wake region of Ahmed body, with variable base slant angle was studied by Ahmed, *et al*. (1984). They observed that the time-averaged structure of the wake consists of a pair of horseshoe vortices, situated one above another in the separation bubble, and of trailing vortices coming off the slant side edges. Ahmed, *et al*. (1984) also reported an explanation of the interactions of these structures and the description of the surface flow features on

* Corresponding Author, E-mail: bsahin@cu.edu.tr

the rear slanted and vertical surfaces. Lienhart, *et al*. (2000) performed more detailed experiments on the same body at a somewhat lower velocity. They measured the time-averaged and fluctuating velocities using LDA, hot wire and obtained surface oil-flow visualization for two different rear vehicle body slant angles (α = 25° and 35°). Their results show the differences in the flow structures for two different slant angles considered. Duell and George (1999) investigated the unsteady near wake flow of a bus-like ground vehicle based on the Ahmed body, with a rear slant angle of 90°. They reported that there are two periodic processes in the wake flow region corresponding to the dimensionless frequencies at Strouhal numbers of 0.069 and 1.157. The lower Strouhal number value was attributed to the periodic interaction of the upper and lower partitions of the ring like vortex in the near wake. The higher value was found to be associated with the vortex shedding process in the shear layer. They also investigated the effects of a base cavity on the unsteady base pressure and concluded that the base pressure increases with increasing cavity depth. Sphon and Gillieron (2002) studied the complex flow phenomena occurring around the Ahmed model via the flow visualization water tunnel based technique. They found that the near-wake flow was dominated by a set of counter-rotating trailing vortices, which was bounded by a central separation bubble that enclosed a flow reversal region. Although the Reynolds number based on the incoming flow velocity and the length of the bluff body was about 3×10^4, it was concluded that the position and topology of the flow structure are in good agreement with the previous studies and the use of low speed water tunnels in combination with flow visualization appears to be a useful tool to complete wind tunnel studies. Sims-Williams and Duncan (2003) investigated the unsteady wake of the Ahmed model both experimentally and numerically. They found that the experimental results and CFD results both revealed that a quasi-two-dimensional vortex shedding type structure occurs emerging from the bottom of the model base. This results in a semi periodic build up and collapse of the near wake and produces a symmetric oscillation. The period of this phenomenon corresponds to a Strouhal number of approximately 0.5. Han (1989) used Reynolds-averaged Navier-Stokes equations (RANS) to simulate the flow around the Ahmed model and reported that the flow structures were in good agreement with those found in experiments. He also concluded that the flow at the slant angle of the body larger than 30° becomes highly unsteady and can not be predicted using steady-state RANS simulations. Krajnovic and Davidson (2003) analyzed the flow around a simplified bus model in order to using large-eddy simulation (LES). Mechanisms of the formation of flow structures, instantaneous and time-averaged flow features were verified with the previous experimental results. The computed aerodynamic forces and their time history were used to reveal the characteristic frequencies of the flow motion around the body. They also reported that at the Reynolds number of 0.21×10^6, based on the model height and the incoming velocity, the flow produced features and aerodynamic forces relevant for the higher Reynolds numbers. Xu and Guo (2003) investigated the dynamic behavior of the high-sided road vehicle subjected to a sudden crosswind gust. it is numerically demonstrated that the road vehicle running on the road having average condition may have an accident with relatively smaller speed comparing to the road having very good condition for a similar crosswind gust. Kim, *et al*. (2005) demonstrated that variations of turbulent boundary layer thickness altered the structure of the flow around the rectangular prism.

The flow around single wall mounted cube in a fully developed channel flow was investigated experimentally by Martunizzi and Tropea (1993) and Hussein and Martinuzzi (1993). In their studies the major flow features; the horseshoe vortex developed at the windward face, the arc-shaped vortex in the wake of the cube and the flow separations on the top and side faces of the cube were well documented including a detailed description of the Reynolds stresses and higher

order moments. A number of computational studies have been carried out to examine the capability of different unsteady RANS and LES turbulence models for flow around a square cylinder (Bosch and Rodi 1998, Rodi 1998, Lee 1999). Krajnovic (2002) provided a detailed flow visualization of a surfaced-mounted cube. The differences between the flow around a vehicle and a surface mounted cube were examined by Krajnovic and Davidson (2001).

The aim of the present work is to investigate the external aerodynamics of a rectangular body with the ground effect and to provide an experimental database that can be used as a benchmark to validate CFD simulations and to have a comparison with the flow structure around a real bus model by other researchers.

2. Experimental arrangement

Experiments were conducted in a closed-loop, open surface water channel. The test-section had a rectangular cross-section of $0.75\times1\ m^2$ and a length of 8 m. The flow was driven by a 15 kW centrifugal pump having a variable speed controller. Before entering the test chamber, the flow passed through a settling reservoir, honeycomb and a contraction. Side and bottom walls of the test section were equipped with 15 mm thick Plexiglas for optical access. The mean velocity was uniform and average turbulent intensity was less than 0.5% in an empty test section. For the present experiments, a 2 m long ground board mounted 0.1 m above the bottom wall of the test section was used to simulate ground effects. The ground board covered the cross section of the tunnel and had a rounded leading edge to avoid flow separation. The schematic view of the experimental configuration was given in Fig. 1. The length, height and width of the model were $L = 175$ mm,

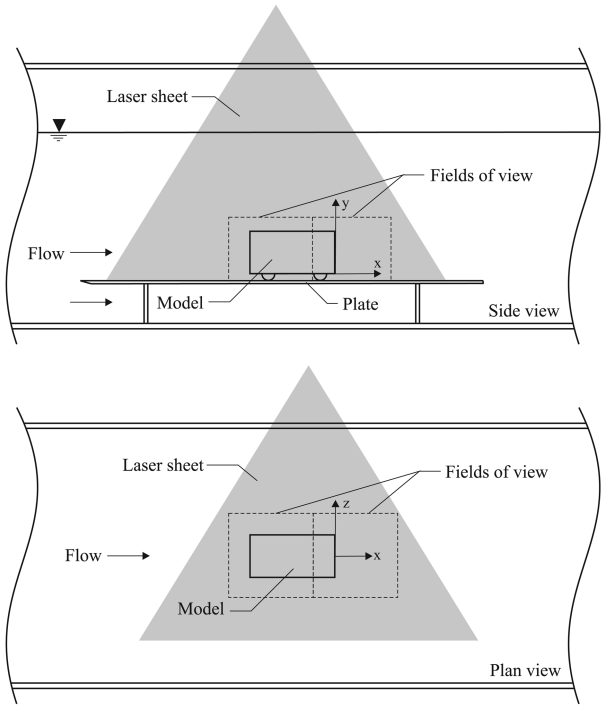

Fig. 1 Schematic of the experimental system

H = 66 mm, and W = 56 mm, respectively. The gap between the ground board and the bottom surface of the model was 9mm. The free stream velocity was U = 0.183 m/s which corresponded to the Reynolds number $Re_H = 1.2\times10^4$ based on the model height.

The velocity fields were measured by Dantec PIV system which consisted of a dual-head Nd:YAG laser, a high resolution CCD camera, a synchronizer and optics. The Nd:YAG laser provided a maximum output energy of 120 mJ per pulse. The CCD camera had a spatial resolution of 1024×1024 pixels with a maximum frame rate of 15 frames per second. The time interval between pulses was 1.2 ms. The camera was equipped with a lens of a focal length of 60 mm. The Nd:YAG laser and CCD camera were synchronized using a Dantec FlowMap Processor. The flow was seeded with silver-coated spherical particles of 12 μm in diameter. The measuring plane was illuminated by a laser sheet generated from the Nd:YAG laser system. The thickness of the laser sheet was approximately 2 mm. The time interval and the laser sheet thickness were selected such that the maximum amount of particle displacement in the interrogation window was obtained. Instantaneous velocity vector fields were generated using a cross-correlation technique between successive particle images. The interrogation window size was 32×32 pixels with 50% overlap providing 3844 (62×62) velocity vectors over the entire field of view plane. The fields of view around the model were 14.73 cm×14.73 cm in size both in the vertical and horizontal view planes. To determine the time-averaged mean flow structure, 300 instantaneous velocity fields were measured. These instantaneous velocity fields were averaged to obtain spatial distributions of the mean velocity and turbulence statistics. Qualitative flow visualization experiments were also performed by injecting fluorescence dye from the leading edge of the model using home made mechanisms.

3. Results and discussion

3.1. Time-averaged velocity field

PIV measurements were performed on the vertical and horizontal symmetry planes. Fig. 2 presents the time-averaged velocity vectors map $<V>$, patterns of streamlines, $<\psi>$ and corresponding vorticity contours, $<\omega>$ along the model on the vertical symmetry plane. As the free stream flow approaches to the model, the speed of the flow particularly along the central axis deteriorates gradually and hence a stagnation point appears at the central point of the model. The time-averaged patterns of streamlines are diverged rapidly as the free stream flow takes place in close region of the front surface of the model and hence the approaching flow is further divided into two main flows. The division starts from the half-saddle point of attachment, S_{ab} indicated by a small arrow in Fig. 2, located on the upstream surface of the model. One part of the flow is oriented towards the bottom surface and the other part is oriented towards the roof surface of the model. Animations of 300 instantaneous images indicate that, this saddle point of attachment, S_{ab} moves upward and downward directions in random motion. As soon as the flow passes the sharp corners, the flow begins to separate rapidly. The upper part of flow is separated starting from the sharp leading top edge and hence a large reverse flow region is formed. The leading edge shear layer is reattached to the model roof surface as indicated by a half-node of attachment, N_a. Here, the centers of the foci, saddle points, the node of attachment and the line of divergence are designated as F, S, N_a and, L_d, respectively. The distance of the reattachment point to the leading edge is $x/H = 1.3$ which corresponds to 48% of the model length. This shear layer reattachment directly influences the

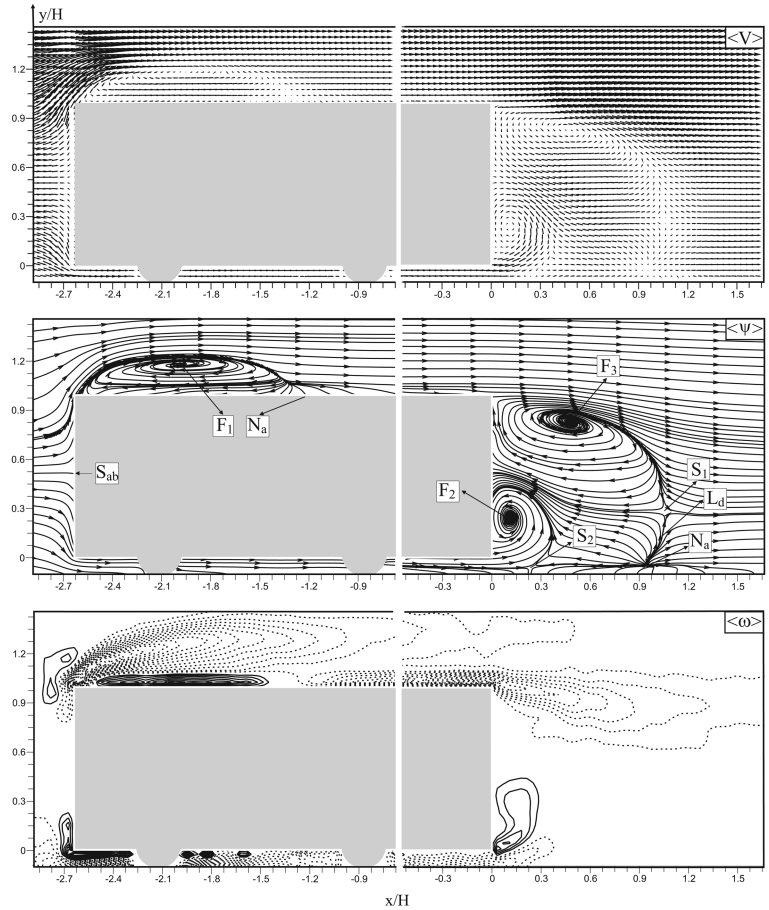

Fig. 2 Patterns of time-averaged velocity vectors map, $<V>$, streamlines, $<\psi>$ and vorticity contours, $<\omega>$, minimum and incremental values of vorticity are $<\omega_{min}> = \pm 4s^{-1}$ and $\Delta<\omega> = 4s^{-1}$

drag on the model (Higuchi, *et al*. 2006). Patterns of streamlines, $<\psi>$ along the vertical symmetry plane indicates that a well defined focus, F_1 occurs on the roof surface of the model. The distance of the focus, F_1 to the leading edge of the model is $x/H = 0.66$. The model induces a recirculating flow zone and an asymmetric pair of vortices. Downstream of the model, separation occurs and two shear layers are developed which interact with each other in the near wake region. Regions of positive and negative vorticity contours are created by the upperbody shear layer and the underbody shear layer, respectively. The length of the underbody shear layer is shorter than the length of the upperbody shear layer as a result of the ground effect. Jet like flow emerging from the narrow gap between the lower wall of the model and ground surface creates the base corner vortex. In the wake region, two recirculatory bubbles are observed, one located above the other, and they rotate in the sense of opposite directions. The bubble rotating in clockwise direction interacts with the upper region of the vertical base, while the lower bubble, which rotates in the opposite direction, covers the bottom surface. The upsweep flow in the recirculatory region is clearly identifiable. The saddle point, S_1 defines the size of the wake region. The time-averaged velocity vectors $<V>$ map and the corresponding patterns of streamlines $<\psi>$ clearly indicate the location of the saddle point which is

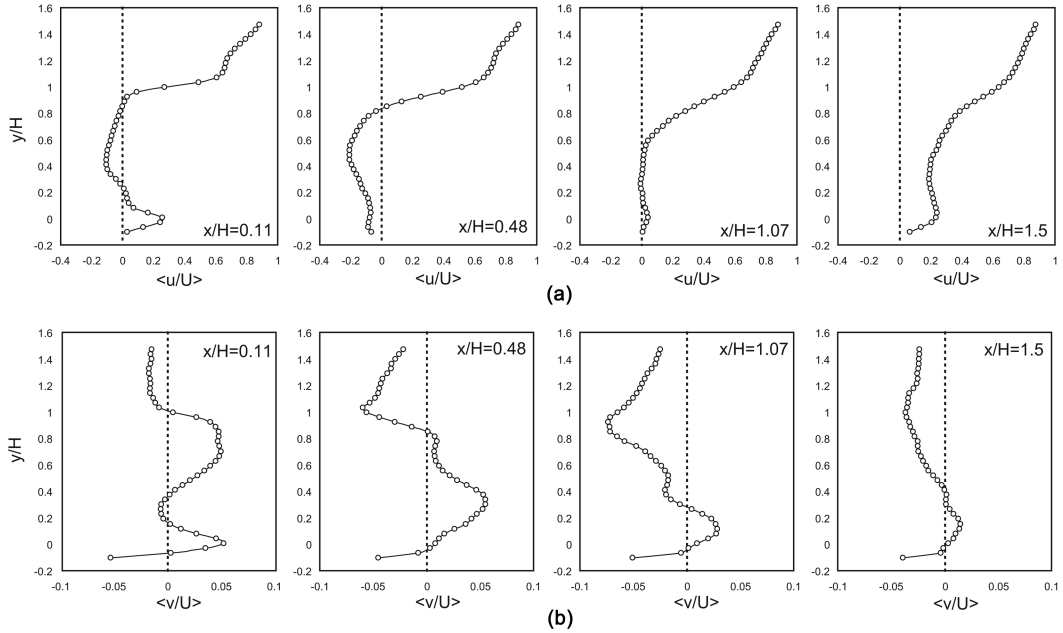

Fig. 3 Velocity profiles of the flow in the vertical symmetry plane in the wake region. (a) Dimensionless streamwise velocity component, $<u/U>$, (b) Dimensionless spanwise velocity component, $<v/U>$.

far from the model base with a distance of $x/H = 1.07$ which corresponds to 61% of the model height. Between nodal point of attachment, N_a and saddle point, S_1, a line of divergence, L_d takes place. A pair of foci, F_2 and F_3 are observed near the bottom and upper edges of the model with distances of $x/H = 0.11$ and 0.48, respectively. Nodal point of attachment, N_a is also evident as seen in Fig. 2.

Fig. 3 shows the time-averaged normalized velocity profiles in the wake region downstream of the model at the selected locations on the vertical symmetry plane. Here, velocity components are normalized with the free stream velocity, U. Fig. 3(a) shows the streamwise velocity profiles, $<u>/U$ at different downstream locations behind the model. The wake flow downstream of the model is reversed causing a negative velocity in between $x/H = 0.11$ and $x/H = 1.07$. The maximum reversed velocity in the recirculatory flow region is approximately one-fifth of the free stream velocity, U. The location of the maximum reversed velocity coincides with the midsection of the model. At the first measuring station ($x/H = 0.11$) streamwise velocity takes negative values between $y/H = 0.2$ and $y/H = 1$ which corresponds to the boundaries of the model. Because of the jet flow occurring between the ground and the bottom surface of the model, streamwise velocity increases in this region. The rate of increase in the streamwise velocity across the shear layer at the upper part of the model is due to the entrainment of wake and the core flow regions. The jet flow emanating from the narrow gap between the ground board and the bottom surface of the model travels towards the mid-section of the model and later interacts with the reversed flow which arising from the top trailing edge and loses its strength rapidly. As a result of this interaction, a negative velocity region occurs below the level of $y/H = 0.8$ at the measuring section of $x/H = 0.48$. Since the third measuring section, $x/H = 1.07$ correspond to the saddle point, streamwise velocity distribution in the spanwise direction does not indicate any negative velocity value. Fig. 3b displays the time-averaged

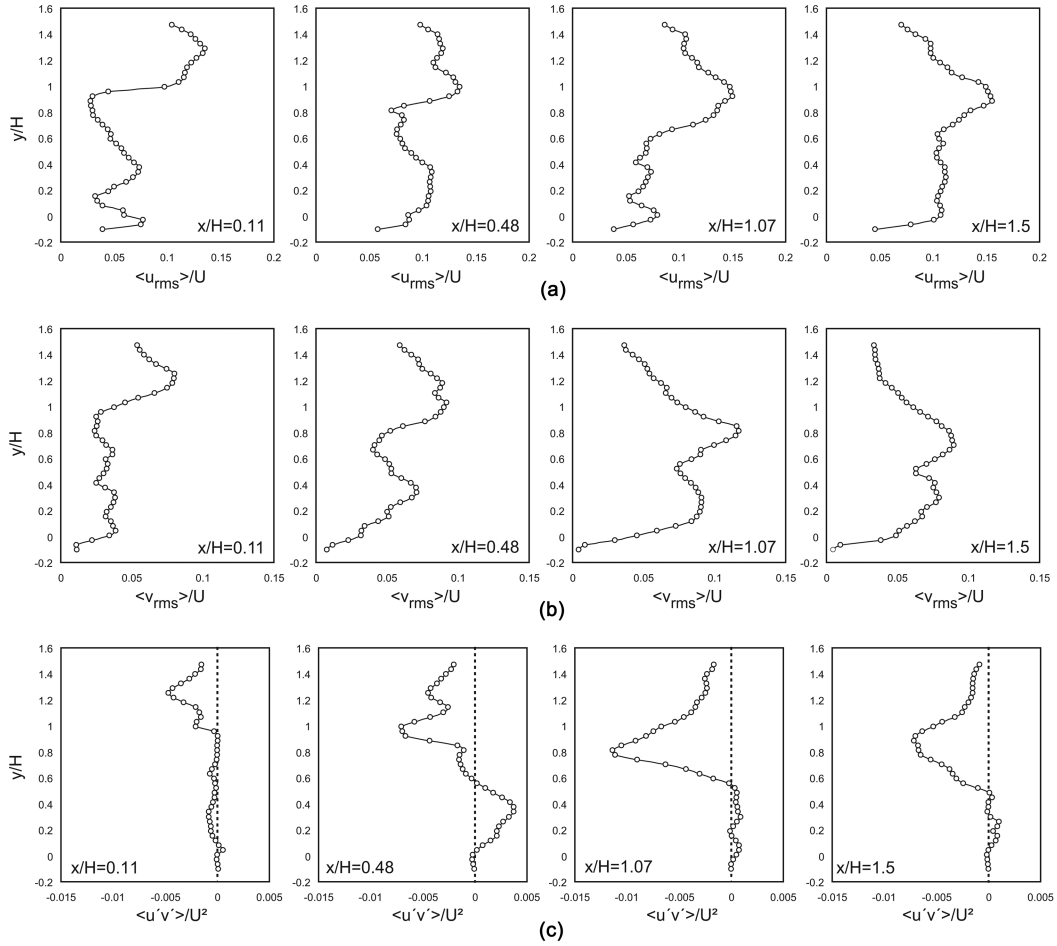

Fig. 4 Profiles of turbulence properties in the vertical symmetry plane in the wake region . (a) Root mean square of streamwise velocity fluctuations, $<u_{rms}>/U$, (b) spanwise velocity fluctuations, $<v_{rms}>/U$, (c) Reynolds stress correlations, $<u'v'>/U^2$.

spanwise velocity profiles, $<v>/U$ at the symmetry plane. Rapid changes in velocity profiles occur along the lateral directions of shear layers. These velocity profiles reveal that there is an intense shear throughout the velocity field. Positive spanwise velocity in the near wake indicates the upsweep flow. The maximum upsweep velocity is 0.07 times the free stream velocity, U. The velocity field viewing both distributions of the velocity components, u and v present that, the flow field is not symmetric due to the ground effect. Fig. 4 presents the profiles of the root mean square of streamwise and spanwise velocity components, $<u_{rms}>/U$ and $<v_{rms}>/U$ normalized by the free stream velocity, U and Reynolds stress correlation, $<u'v'>/U^2$ normalized by the square of the free stream velocity in the central region of vertical plane. The locations of peak values of $<u_{rms}>/U$ and $<v_{rms}>/U$ take place along the upperbody and underbody shear layers. The magnitude of the root mean square of streamwise velocity fluctuations, $<u_{rms}>/U$ shown in Fig. 4(a) are higher in the upperbody shear layer than that of in the underbody shear layer as a result of the ground effect. The peak value of $<u_{rms}>/U$ in the upperbody shear layer is approximately 0.16 at $x/H = 1.5$. The root

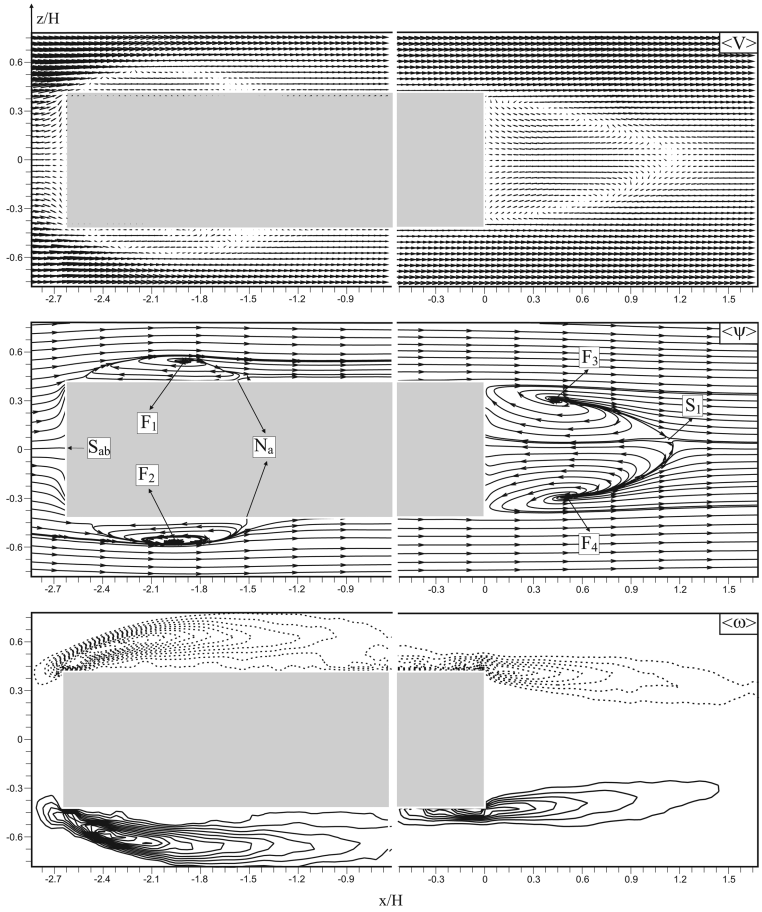

Fig. 5 Patterns of time averaged velocity vectors map $<V>$, streamlines, $<\psi>$ and vorticity contours $<\omega>$, minimum and incremental values of vorticity are $<\omega_{min}> = \pm 4s^{-1}$ and $\Delta<\omega> = 4s^{-1}$

mean square of cross stream velocity components, $<v_{rms}>/U$ presented in Fig. 4(b) shows a similar trend. The maximum value of $<v_{rms}>/U$ is approximately 0.12 at $x/H = 1.07$ which is smaller than the corresponding value of $<u_{rms}>/U$ at the same location. Profiles of the Reynolds stress correlation, $<u'v'>/U^2$ are shown in Fig. 4(c). The maximum value of Reynolds stress correlation, $<u'v'>/U^2$ appears along the upperbody shear layer with a magnitude of 0.011 at $x/H = 1.07$. Magnitude of Reynolds stress correlations, $<u'v'>/U^2$ along the underbody shear layer are smaller comparing to the upperbody shear layer.

The time-averaged velocity vectors map, $<V>$ patterns of streamlines, $<\psi>$ and corresponding vorticity contours, $<\omega>$ on the horizontal symmetry plane are exhibited in Fig. 5. The main features of the flow in this plane are two shear layers originating from the sharp leading side edges of the model, and the reversed flow region downstream of the model. As the bifurcating streamlines of the incoming flow approaching to the front surface of the model, a half-saddle point of attachment, S_{ab} appears on the front surface of the model. The flow is separated from the vertical side edges and formed two recirculatory flow regions on both side walls of the model. The separating and reattaching shear layers and the recirculating flow within the separation bubbles are clearly seen

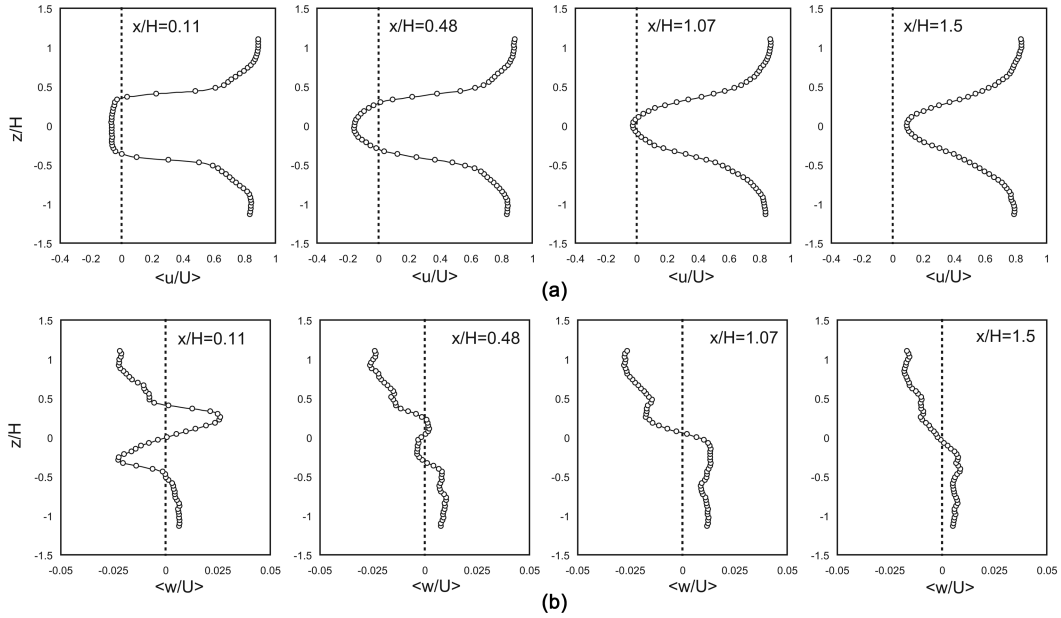

Fig. 6 Velocity profiles of the flow in the horizontal symmetry plane in the wake region. (a) Dimensionless streamwise velocity component, $<u/U>$, (b) Dimensionless spanwise velocity component, $<w/U>$.

from the streamline patterns in Fig. 5. Regions of high vorticity contours define the side wall shear layers. The distance of the reattachment points to the leading edge of the model is about $x/H = 1.06$. A well defined pair of foci, F_1 and F_2 are observed near the side walls of the model which are far from the leading edge with distances of $x/H = 0.74$. In the wake region at the rear part of the model, a pair of similarly sized recirculation region is identified. These two shear layers extend approximately to the same downstream location. A pair of identical foci F_3 and F_4 and a saddle point, S_1 is observed in the wake region. The distances of these points, F_3, F_4 and S_1 to the vertical model base are $x/H = 0.45$, 0.45 and 1.13, respectively.

Fig. 6 presents the time-averaged velocity profiles in the horizontal symmetry plane of the near wake of the model. The streamwise velocity profiles, $<u>/U$ are shown in Fig. 6(a). Similar to the vertical symmetry plane data shown in Fig. 3(a), the reversed flow region occurs resulting in a negative streamwise velocity, u beginning from the rare surface of the model up to a point with a distance of $x/H = 1.07$. The maximum upstream value velocity in the wake region is 0.16 times the free stream velocity, U. Fig. 7 shows profiles of the root mean square of streamwise and spanwise velocity components, $<u_{rms}>/U$, $<v_{rms}>/U$ and the corresponding Reynolds stress correlations, $<u'v'>/U^2$ in the central region of the horizontal plane. The distributions of the root mean square of streamwise velocity fluctuations, $<u_{rms}>/U$ shown in Fig. 7(a) indicate two maxima at two different locations along the lateral direction which correspond to the edge shear layers and have a symmetrical structure. The fluctuations of the cross stream velocity components, $<w_{rms}>/U$ in the lateral direction shown in Fig. 7(b) reveal that the values of $<w_{rms}>/U$ in upperbody shear layers are bigger than that of in underbody shear layer. Profiles of the Reynolds stress correlation, $<u'v'>/U^2$ shown in Fig. 7(c) indicate that the peak values of the Reynolds stress correlations, $<u'v'>/U^2$ occur along the shear layers emerging from the both sides of the trailing edges.

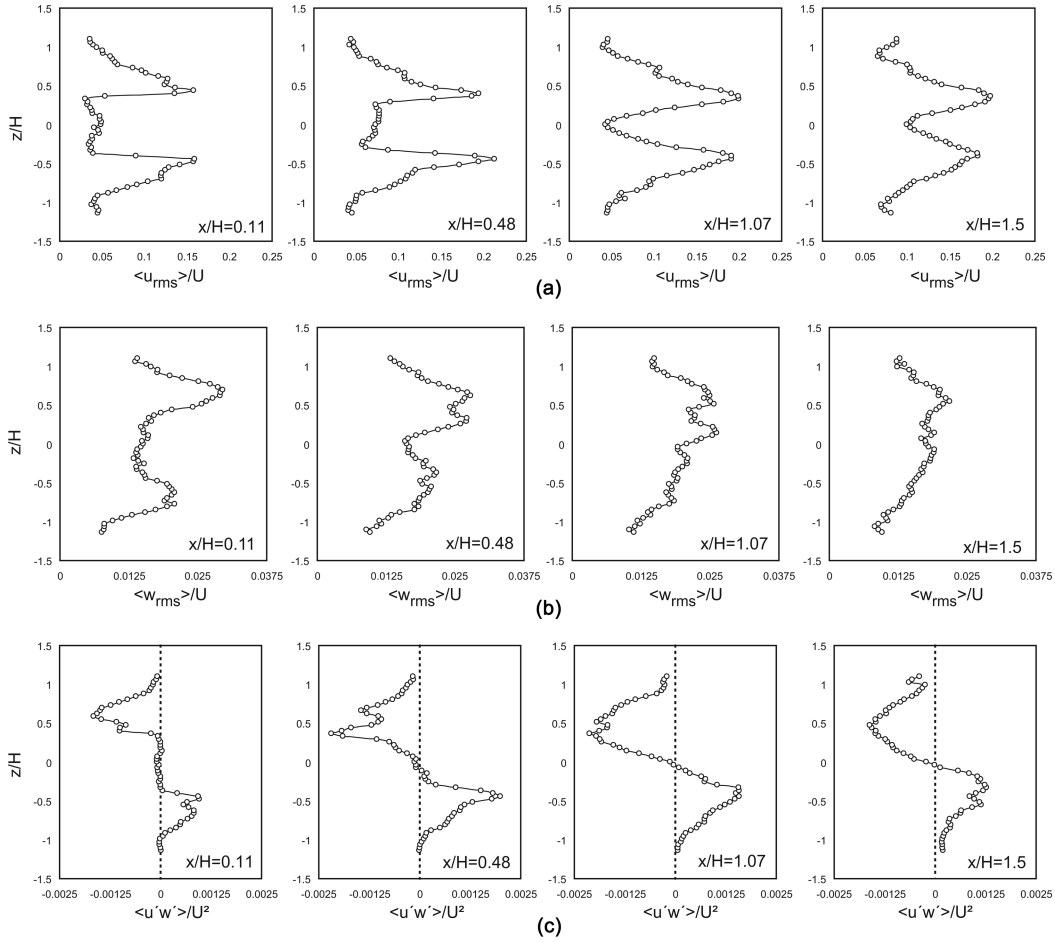

Fig. 7 Profiles of turbulence properties in the horizontal symmetry plane in the wake region. (a) Root mean square of streamwise velocity fluctuations, $<u_{rms}>/U$, (b) spanwise velocity fluctuations, $<v_{rms}>/U$, (c) Reynolds stress correlations, $<u'v'>/U^2$.

3.2. Instantaneous velocity field and flow visualization

Fig. 8 presents the streamlines instantaneous flow patterns along the top roof of the model on the vertical symmetry plane obtained by the PIV technique. The instantaneous velocity vectors map, V and the corresponding stream lines, ψ clearly presents that the large-scale swirling patterns of velocity vectors are evident near the roof surface of the model. These circulatory flow patterns interact severely with the surface of the model in random mode. As soon as the reattachment occurs, swirling patterns of the velocity vector disappears. The time-averaged flow data presented in Fig. 2 indicates that reattachment occurs at $x/H = -1.35$. On the other hand animation of 300 instantaneous velocity vector fields reveals that, the location of the reattachment point moves in forward and backward directions in an unsteady manner. The instantaneous flow streamlines structures along the roof of the model present the generation of additional vortices comparing to the time-averaged flow data. The instantaneous velocity vectors map, V and the patterns of stream lines,

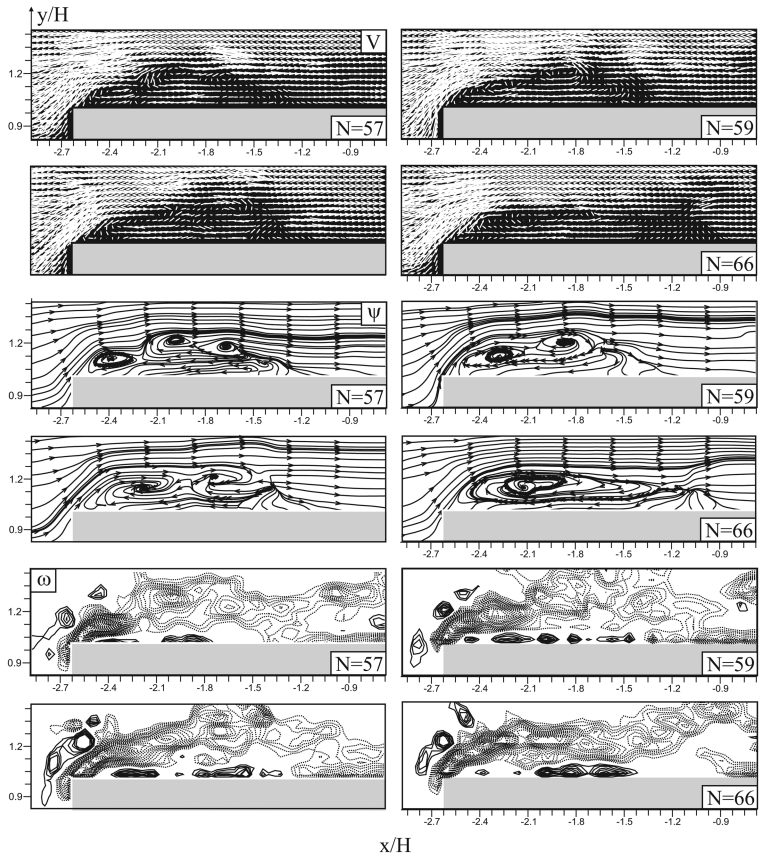

Fig. 8 Instantaneous flow fields on the vertical symmetry plane on the top roof of the model

ψ present three different vortices. Combination of these vortices creates a well defined single vortex occupying the whole are of the wake flow region with an expansion in the flow direction. Contours of vorticity, ω show that the concentration of vortices occurs along the shear layer. As soon as the wake region expands in the flow direction with a single focus, the vortex elongates in the flow direction along the shear layer. The instantaneous flow structure in the wake region downstream of the model on the vertical symmetry plane shown in Fig. 9 indicates that, swirling patterns of velocity vectors take place along the inner regions of the upperbody shear layer. On the other hand, well defined large-scale swirling patterns of velocity vectors are evident on the bottom edge of the vertical base of the model. The positive vortex induced in the under body shear layer grows in size, elongates and loses its strength as shown in the first three frames. The point of attachment on the ground surface travels forward and backward in the flow direction in unsteady mode. Shear layers emanating from the upperbody and lowerbody surfaces cause complex flow field which consists of a number of vortices that move randomly in time and space. Fig. 10 shows the instantaneous flow field downstream of the model in the horizontal symmetry plane. The generation of additional vortices is clearly visible. Circulatory flow motions which increase the rate of entrainment between the wake and the main flow regions take place along the both shear layer. Namely, well defined Kelvin-Helmholtz vortices occur. Topology of the flow structure clearly shows that the size of the wake flow region changes randomly.

The spectra of streamwise velocity fluctuations obtained using FFT analysis for three selected

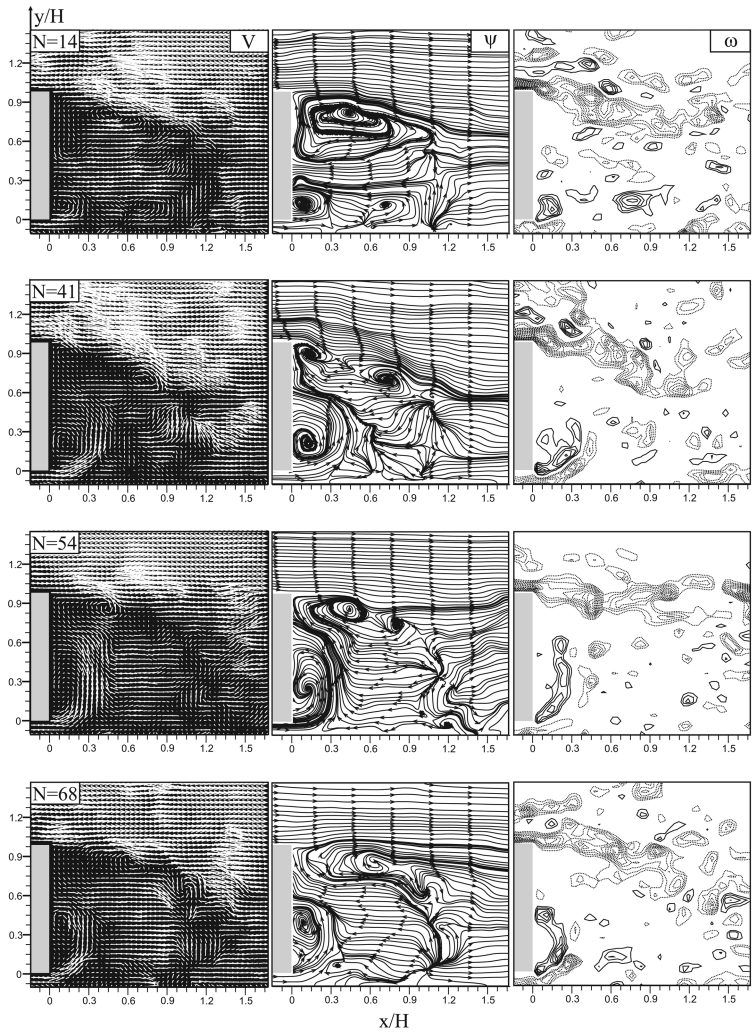

Fig. 9 Instantaneous flow fields in the wake region on the vertical symmetry plane

points in the vertical symmetry plane are shown in Fig. 11. The location of the selected points are in the lower shear layer ($x/H = 0.25$, $y/H = 0.4$), in the upper shear layer ($x/H = 0.22$, $y/H = 1.09$) and close to the saddle point ($x/H = 0.99$, $y/H = 0.25$) in the wake region. The dominant frequency of $f = 0.414$ Hz at the third point close to the saddle point corresponds to the Strouhal number $St = fH/U = 0.153$ (based on the model height H and the free steam velocity U) and is consistent with experimental, Duell and George (1999) and numerical, Krajnovic and Davidson (2001) results of the flow around bus like ground vehicle body. Duell and George (1999) measured the Strouhal number as $St = 0.155$ at the point close to the free stagnation point and they concluded that this peak indicates the vortex pairing close to the free stagnation point.

The dye flow visualization of separating shear layers on the upper surface of the model and on the side walls are shown in Figs. 12(a) and (b), respectively. Shear layer instability waves were clearly identifiable both in vertical and horizontal symmetry planes. Flow visualization both on the roof of the model and around the vertical side wall displays identical flow structures due to the

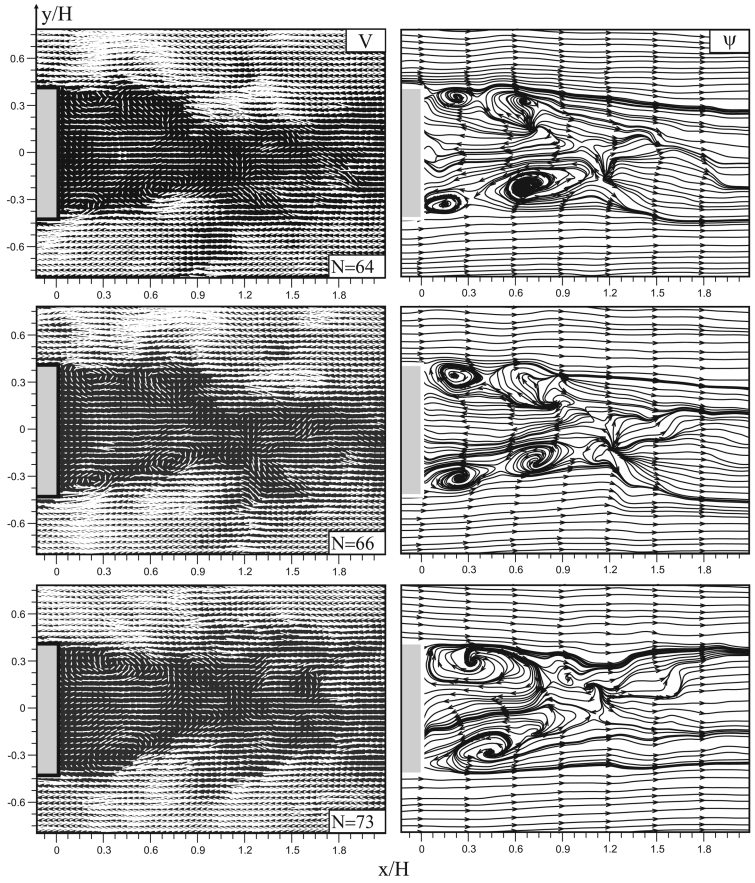

Fig. 10 Instantaneous flow fields in the wake region on the horizontal symmetry plane

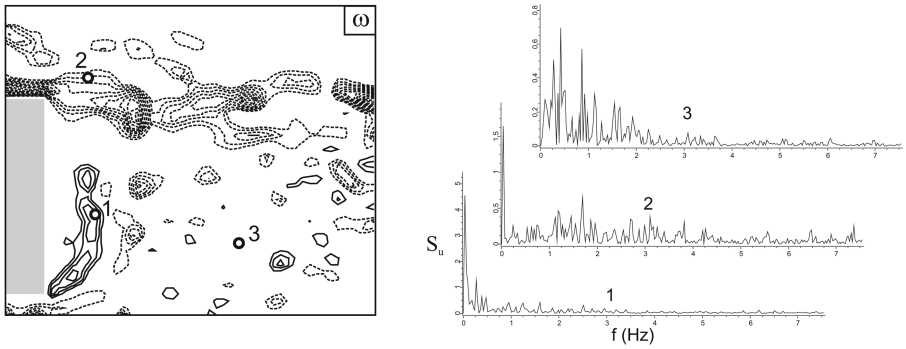

Fig. 11 The spectrum of streamwise velocity fluctuations for selected points downstream of the model

geometrical similarity. Quantitative data obtained by PIV shown in Fig. 8 and qualitative flow data obtained by dye flow visualization presented in Fig. 12(a) are in good agreement with each other. In both cases, a well defined vortex appears as soon as separation starts and expands in size while revolving further downstream. Fig. 13 presents the dye flow visualization in the wake region on the vertical symmetry plane. A well-defined ring type vortex clearly appears on the lower side of the

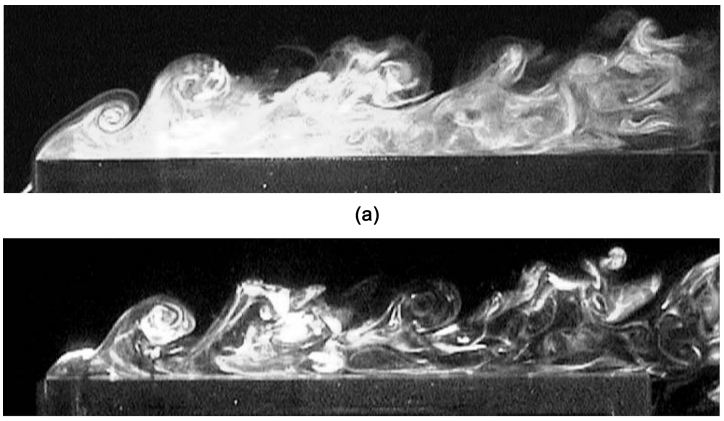

Fig. 12 (a) Dye flow visualization on the model roof in the vertical symmetry plane. (b) Dye flow visualization on the lateral vertical side in the horizontal symmetry plane

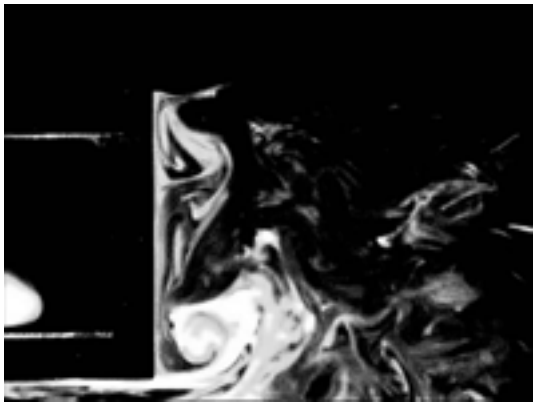

Fig. 13 Dye flow visualization in the vertical symmetry plane in the wake region

rear wall of the model due to the jet like flow emerging underbody of the model.

4. Conclusions

The flow structure around a three–dimensional rectangular body has been investigated experimentally using PIV measurements and the flow visualization technique. Although the geometry of the model investigated in this study is relatively simple, the flow around it appears to be very complex. At the vertical symmetry plane, a large reverse flow region is observed on the model roof. The distance of the reattachment point to the leading edge is $x/H = 1.3$. In the wake region downstream of the model, two recirculatory bubbles are developed in opposite directions. Shear layer emanating from the top side of the model dominates the wake region downstream of the model with a larger length scale comparing to the underbody shear layer. The rates of fluctuations are higher along the upper shear layer due to the high rate of momentum. Jet like flow emerging from the narrow gap between the lower wall of the model and ground surface penetrate into the wake region creates the base corner vortex.

In the horizontal symmetry plane, two reversed flow regions investigated around both vertical side

walls and in the wake region downstream of the model. The separated leading edge shear layers reattach approximately at the same locations both on the roof and vertical side walls of the model due to the geometrical similarity. Instantaneous flow data show that, these reattachment points move forward and backward in the flow direction in an unsteady motion. Separated flow region consist of well defined vortices interact with the surface continuously.

The PIV velocity field measurements are available as a test data set for the validation of numerical simulations.

Acknowledgments

The authors would like to acknowledge the financial support of the Office of Scientific Research Projects of Cukurova University for funding under contract No: MMF2006D32.

References

Ahmed, S.R. *et al*. (1984), "Some salient features of the time averaged ground vehicle wake", SAE Paper No. 840300.

Bosch, G. and Rodi W. (1998), "Simulation of vortex shedding past a square cylinder with different turbulence models", *Int. J. Numer. Methods Fluids*, **28**, p. 601-616.

Duell, E.G., George, A.R. (1999), "Experimental study of a ground vehicle body unsteady near wake", SAE Paper No. 1999-01-0812.

Han, T. (1989), "Computational analysis of three-dimensional turbulent flow around a bluff body in ground proximity", *AIAA J*., **27**(9), pp. 1213-1219.

Higuchi, H. *et al*. (2006), "Axial flow over a blunt circular cylinder with and without shear layer reattachment", *J. Fluids Struct*., **22**, pp. 949-959

Hussein, H.J. and Martinuzzi, R.J. (1993), "Energy balance of turbulent flow around a surface mounted cube placed in a channel", *Phys. Fluids*. **8**(3), 764-780.

Krajnovic, S. (2002), "Large eddy simulation of the flow around a three-dimensional bluff body", PhD thesis, Dept. of Thermo and Fluid Dynamics, Chalmers Univ. of Tech., Gothenburg, Sweden.

Krajnovic, S. and Davidson, L. (2001), "Large eddy simulation of the flow around a ground vehicle body", In *SAE 2001 World Congress*, SAE Paper 2001-0-10702, Detroit Michigan, USA.

Krajnovic, S. and Davidson, L. (2003), "Numerical study of the flow around a bus-shaped body", *ASME J. Fluids Eng*., **125**, pp. 500-509.

Lee S., (1998), "Numerical study of wake structure behind a square cylinder at high Reynolds number", *Wind Struct., An Int. J*., **1**(2), pp. 127-144.

Lienhart, H. *et al*. (2000), "Flow and turbulence structures in the wake of a simplified car model (Ahmed model)", *In DGLR Fach Symp. der AG STAB*.

Martinuzzi, R. and Tropea C. (1993), "The flow around surface-mounted, prismatic obstacles placed in a fully developed channel flow", *ASME J. Fluids Eng*., **115**, pp. 85-91.

Rodi W. (1998), "Comparasion of LES and RANS calculations of the flow around bluff bodies", *J. Wind Eng. Ind. Aerodyn*., **69**, 55-75.

Sims-Williams, D.B. and Duncan B.D. (2003), "The Ahmed model unsteady wake: experimental and computational analyses", SAE Paper No. 2003-01-1315.

Spohn, A. and Gillieron, P. (2002), "Flow separations generated by a simplified geometry of an automotive vehicle", *in: Congress IUTAM Symposium on Unsteady Separated Flows*, Toulouse, France

Xu Y.L. and Gou W.H. (2003), "Dynamic behaviour of high-sided road vehicles subjected to a sudden crosswind gust", *Wind Struct*., *An Int. J*., **6**(5), pp. 325-346.

Kim C.K., Ji H.S. and Seong S.H. (2005), "Effects of turbulent boundary layerthickness on flow around a low-rise rectangular prism", *Wind Struct*., *An Int. J*., **8**(6), pp. 455-467.

CC